Analytical Methods

ROYAL SOCIETY OF CHEMISTRY

PAPER

View Article Online
View Journal | View Issue

Cite this: *Anal. Methods*, 2021, **13**, 2092

Investigating the effect of 6-mercaptohexanol on the performance of a biosensor based on nanosurface energy transfer between gold nanoparticles and quantum dots†

Qizhen Lai,[a] Yucheng Liu,[b] Lan Ge,[a] Yeling Yang,[a] Xinghu Ji*[a] and Zhike He *[a]

Received 4th February 2021
Accepted 25th March 2021

DOI: 10.1039/d1ay00209k

rsc.li/methods

Nanosurface energy transfer (NSET)-based sensors have been widely developed using various pairs of nanomaterials including gold nanoparticles (AuNPs) and quantum dots (QDs). However, a low signal to background ratio is one of the most important problems that researchers are continually trying to solve. Herein, we present a 6-mercaptohexanol (MCH) modified MCH/DNA-Au-QD sensor for the detection of nucleic acids and MUC1. Interestingly, an unexpected effect of MCH was found in enhancing the fluorescence recovery ratio, therefore yielding a higher signal to background ratio. Through further investigation, we perceive the enhancement as a result of lowering of the NSET efficiency between free DNA-AuNPs and free DNA-QDs, which arises from the stretching of adsorbed DNA on the surface of AuNPs. The employment of MCH endowed the sensor with a wider linear range from 5 nM to 120 nM and a relatively lower LOD of 1.19 nM in nucleic acid detection, outperforming the original DNA-Au-QD sensor. Furthermore, the application of the sensor can be further extended to MUC1 detection. This study offers a better understanding of the NSET process between QDs and AuNPs and also initiates a new approach for the performance optimization of analogous NSET-based sensors.

Introduction

Nanosurface energy transfer (NSET) is a process that involves non-radiative energy transfer from a photoexcited donor to a metal nanoparticle surface in close proximity. Compared with traditional Förster resonance energy transfer (FRET), the relatively new NSET theory regards a nanometric acceptor as a surface dipole rather than a point dipole.[1] Beneficially, according to NSET theory, the energy transfer was effective in a distance range up to 40 nm, breaking through the distance limit (1–20 nm) of traditional FRET and laying the foundation for broader application of NSET in long range systems.[2,3] So far, NSET has been employed in lots of extraordinary research studies, including accurate spectral analysis,[4–7] bioimaging[8–10] and other applications.[11–13]

In terms of NSET-based applications, the appropriate selection of the donor–acceptor pair is crucial. On the one hand, among noble metal nanoparticles, gold nanoparticles (AuNPs) exhibit a broad absorption spectrum and tremendously high extinction coefficient which enables a valid overlap with the emissions of diverse donors,[14] making AuNPs an excellent acceptor. On the other hand, quantum dots (QDs) are at a special advantage when employed as an energy donor in NSET-based applications due to the merits of wide excitation, narrow and symmetrical emission spectra, tunable size along with emission lines, and high quantum yields.[15–19] Hence, AuNPs-QDs can be a competitive donor–acceptor pair, fitting well with NSET theory.[20–22] Benefiting from the remarkable optical properties of these two nanoparticles, AuNPs and QDs have been used in NSET-based biosensors for detection of miRNA[23,24] and metal ions.[25,26] Nevertheless, sometimes these assays suffered from several problems, such as high background due to ineffective energy transfer from SA-coated QDs to AuNPs[23] and a nonlinear standard curve ascribed to the quenching effect of free DNA-AuNPs on free DNA-QDs,[25] both of which have an adverse impact on the signal to background ratio along with reduced sensitivity. The former issue has been wisely settled by introducing another quencher (BHQ2) to lower the background,[23] The latter one, however, has not been fully investigated yet. Therefore, it is meaningful to address the problem for better construction of NSET-based DNA-Au-QD sensors.

It is well known that thiolated oligonucleotides can be easily modified on the surface of AuNPs *via* Au–S bonds. However, the positively charged nitrogenous bases tend to adsorb to the negatively charged AuNP surface, resulting in a low

[a]*College of Chemistry and Molecular Sciences, Wuhan University, Wuhan 430072, China. E-mail: zhkhe@whu.edu.cn; Fax: +86 27-68754067; Tel: +86 27-68756557*

[b]*The Centre of Analysis and Measurement of Wuhan University, Wuhan University, Wuhan, 430072, P. R. China*

† Electronic supplementary information (ESI) available. See DOI: 10.1039/d1ay00209k

hybridization efficiency or recognition capability towards its target. In this circumstance, it is noteworthy that 6-mercapto-1-hexanol (MCH), a small thiol molecule, can be employed as a blocking reagent to minimize the nonspecific adsorption and improve the hybridization efficiency or recognition capability.[27,28] In this work, a simple NSET-based MCH/DNA-Au-QD sensor was constructed for nucleic acid and MUC1 detection. On top of that, we accidentally found that MCH played an additional and important role in avoiding the quenching of free DNA-AuNPs on free DNA-QDs, and the mechanism was further explored. Then, the MCH concentration was optimized to yield a higher signal to background ratio, further producing an enhanced sensitivity and a wider linear range. Moreover, the sensor was applied to the detection of biomarker MUC1 to demonstrate its universality for other target assays.

Experimental section

Materials and reagents

All chemicals of analytical grade were used as received without further purification. Te powder, $CdCl_2 \cdot 2.5H_2O$ and $ZnCl_2$ were purchased from Shanghai Chemical Reagents Company (China). 6-Mercapto-1-hexanol (MCH) and dithiothreitol (DTT) were purchased from Aladdin (China). Tris(hydroxymethyl) aminomethane hydrochloride (Tris), chloroauric acid ($HAuCl_4 \cdot 4H_2O$), trisodium citrate dihydrate, sodium borohydride ($NaBH_4$) and *N*-acetyl-L-cysteine (NAC) were purchased from Sigma-Aldrich (U.S.A.). All solutions were prepared with ultrapure water purified by a Millipore water purification system (18.25 MΩ cm, 25 °C). Human serum samples were provided by the Zhongnan Hospital of Wuhan University (Wuhan, China). Oligonucleotides were synthesized and purified by Sangon Biotechnology Co. Ltd (Shanghai, China). The sequences of the oligonucleotides used are listed in Table S1.†

Instruments

Fluorescence spectra were recorded using an RF-6000 spectrophotometer (Shimadzu, Japan). UV-vis absorption spectra were recorded on a UV-2250 spectrophotometer (Shimadzu, Japan). Transmission electron microscopy (TEM) and high resolution (HR) TEM images were aquired on a JEM-2100 electron microscope (Japan). Dynamic light scattering (DLS) measurements were performed on a Zetasizer instrument ZEN3600 (Malvern, U.K.). Fluorescence decay curves were collected on a FELIX32 system (Photon Technology International, USA).

The synthesis of AuNPs

15 nm AuNPs were synthesized by the standard citrate reduction method.[29] In brief, 5 mL of 1 wt% sodium citrate aqueous solution was rapidly added to a boiling aqueous solution of $HAuCl_4 \cdot 3H_2O$ (100 mL, 0.5 mM). Then the system was allowed to react for 15 min under continuous stirring and refluxing, during which the solution changed from pale yellow to claret-red. Afterwards, the heating was turned off and the solution was allowed to cool to room temperature under stirring, followed by

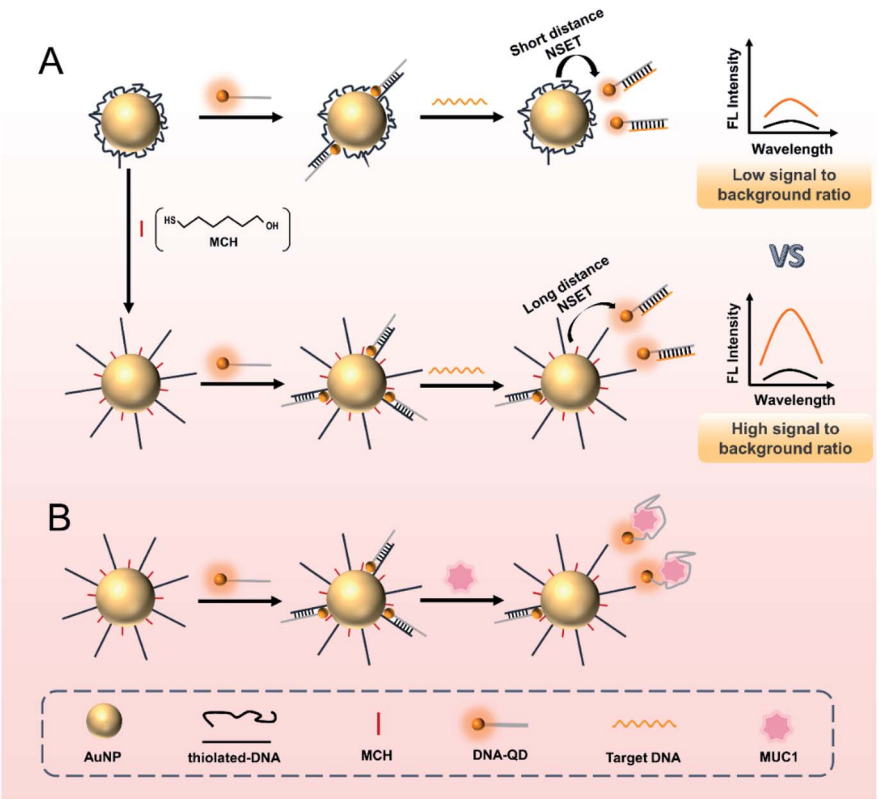

Scheme 1 Schematic illustration of DNA-Au-QDs and the MCH/DNA-Au-QD sensor for (A) nucleic acid and (B) MUC1 detection.

filtering through a 0.22 μm Millipore membrane filter. The prepared AuNPs were stored at 4 °C. The concentration of 15 nm AuNPs was determined based on the Lambert–Beer law with an extinction coefficient of 4.2×10^8 mol^{-1} L cm^{-1} at 520 nm.[30]

The conjugation of AuNPs with thiolated DNA

The freezing method was implemented for the conjugation of AuNPs with thiolated DNA.[31] Typically, thiolated DNA was mixed with the as-prepared AuNPs at a ratio of 200 : 1. The mixture was kept in a laboratory freezer (set at −20 °C) for 2 h until the solution was totally frozen, and then the frozen mixture was thawed at room temperature. To remove the unattached DNA, the mixture was washed thrice with Tris–HCl buffer (10 mM,150 mM NaCl, pH 8.3) *via* centrifugation (13 300 rpm, 20 min).

The MCH treatment of DNA-AuNPs

Briefly, 4 nM DNA-AuNPs were mixed with different concentrations of MCH for 0.5 h at room temperature, followed by centrifuging twice to stop the reaction and remove the excess MCH.

The quantification of DNA strands attached to each AuNP

Typically, FAM (6-carboxyfluorescein) labeled S1 (S1-FAM) was employed to modify AuNPs using the same protocol mentioned above. For MCH/DNA-AuNPs treated with different concentrations of MCH, a final concentration of 20 mM DTT was added and incubated overnight with gentle shaking at room temperature. Afterwards, the resulting AuNP aggregates were precipitated *via* centrifugation and the fluorescence of the supernatant was measured. The concentration of FAM labeled DNA was calculated based on a standard curve plotted using a series of certain concentrations of FAM labeled DNA under the same conditions.

The synthesis of DNA-QDs and QDs

The preparation of DNA-functionalized CdTe:Zn^{2+} QDs was according to our previously published work.[18] Briefly, 20 mg Te powder and 11 mg $NaBH_4$ were quickly dissolved in 1 mL ultrapure water and stirred under oxygen-free conditions in an ice-bath for 5 h to produce the Te precursor. Then, the pH of the solution containing $CdCl_2$ (6.25 mM), $ZnCl_2$ (6.25 mM) and NAC (25 mM) was adjusted to 9.0 to obtain the Cd precursor. Afterwards, 5 μL Te precursor, 0.4 mL Cd precursor and phosphorothioate modified DNA (14 OD) were mixed and transferred into a Teflon-lined-stainless steel autoclave. Then, the reaction system was heated at 200 °C for 29 min to obtain DNA functionalized CdTe:Zn^{2+} QDs. Then the DNA-QDs were purified by using an Amicon Ultra-4 centrifugal filter device. The synthesis of QDs was almost the same, except that no DNA was involved. The concentration of DNA-QDs and QDs was calculated according to a previous study.[32]

The assembly of DNA-AuNPs and DNA-QDs

Briefly, DNA-AuNPs were mixed with DNA-QDs at a ratio of 1 : 20. Afterwards, the mixture was incubated at 25 °C for 1 h, followed by centrifuging thrice at 13 300 rpm to separate the unassembled DNA-QDs. The sediment was redispersed in tris buffer (10 mM, pH 8.3, 150 mM NaCl) and restored at 4 °C.

The detection of nucleic acids and MUC1

The detection of nucleic acids and MUC1 was performed using the MCH/DNA-Au-QD assembly obtained above. For nucleic acid detection, different concentrations of target DNA were mixed with 200 μL MCH/DNA-Au-QD assembly that was composed of S1 and P1 (Table S1†), followed by incubation at 25 °C for 40 min. Then the fluorescence was recorded at an excitation wavelength of 340 nm. The detection of MUC1 was performed exactly the same way by using the MCH/DNA-Au-QD assembly that was composed of S2 and P2 (Table S1†).

Results and discussion

Working principle

The principle of the MCH/DNA-Au-QD sensor for nucleic acid and MUC1 detection is illustrated in Scheme 1. Through the DNA hybridization reaction, AuNPs and QDs were in close

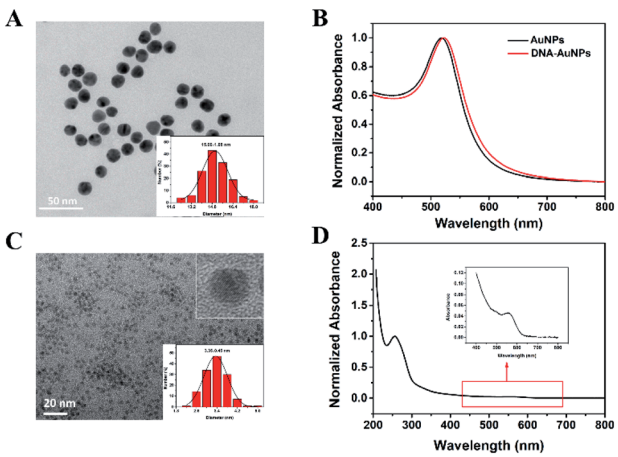

Fig. 1 Characterization of DNA-AuNPs and DNA-QDs. (A) TEM images and size distribution of AuNPs. (B) UV-vis absorbance spectra of AuNPs and DNA-AuNPs. (C) TEM images and size distribution of DNA-QDs. Inset: high resolution TEM image. (D) UV-vis absorbance spectrum of DNA-QDs.

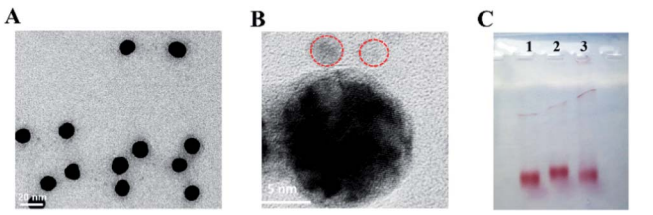

Fig. 2 Characterization of the MCH/DNA-Au-QD assembly. (A) and (B) TEM images of the MCH/DNA-Au-QD assembly. (C) Agarose gel electrophoresis image of DNA-AuNPs (lane 1); MCH/DNA-Au-QD assembly (lane 2); MCH/DNA-Au-QD assembly upon the addition of 120 nM target DNA (lane 3).

Table 1 Fluorescence lifetimes obtained with a biexponential fit of the fluorescence decay curves

Samples	τ_{ave}/ns	R^2
DNA-QDs	27.71	0.955
MCH/DNA-Au-QDs	5.32	0.768
QDs	24.67	0.978
QDs + naked AuNPs	18.22	0.950
QDs + DNA-AuNPs	21.82	0.963
QDs + MCH/DNA-AuNPs	22.77	0.960

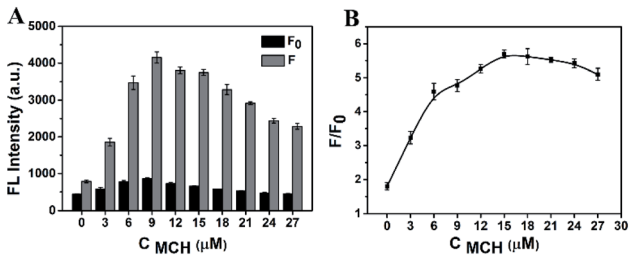

Fig. 3 Optimization of the concentration of MCH. (A) Plots of the signal and background and (B) signal to background ratio (F/F_0) of the MCH/DNA-Au-QD sensor by using MCH/DNA-AuNPs treated with different concentrations of MCH. Concentrations: DNA-Au-QD assembly: 3.5 nM, target DNA: 120 nM.

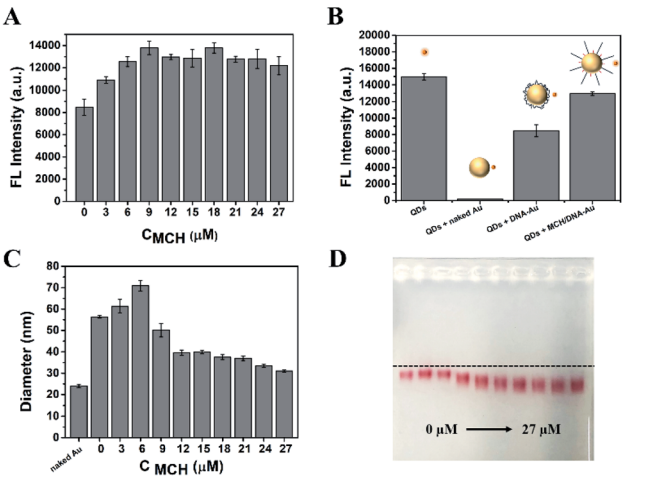

Fig. 4 The influence of MCH on MCH/DNA-AuNPs. (A) Quenching effect: fluorescence intensities of QDs in the presence of MCH/DNA-AuNPs treated with different concentrations of MCH. (B) Fluorescence intensities of QDs in the absence and presence of naked AuNPs, DNA-AuNPs and MCH/DNA-AuNPs. Concentrations: MCH/DNA-AuNPs or AuNPs: 0.5 nM, QDs: 10 nM; reaction time: 1 h. (C) Average hydrodynamic diameter and (D) agarose gel electrophoresis image of MCH/DNA-AuNPs treated with different concentrations of MCH.

proximity in a "head to head" pattern, resulting in the fluorescence quenching of QDs. Crucially, the exposed sticky end of the DNA (or aptamer) modified on QDs served as a recognition unit. Upon addition of the target, DNA-QDs deviated from the surface of AuNPs due to stronger binding affinity with the target, resulting in the proportional recovery of QD fluorescence. More importantly, once the DNA-AuNPs were pretreated with MCH, DNA strands were oriented in an upright position, which allowed the free DNA-QDs to be more distant from the surface of DNA-AuNPs, further weakening the NSET quenching effect of free DNA-AuNPs on free DNA-QDs, and a higher signal to background ratio was achieved.

The characterization of the MCH/DNA-Au-QD assembly

The synthesized AuNPs were monodispersed and around 15 nm in diameter, as shown in the TEM image in Fig. 1A. The UV-vis absorption spectra in Fig. 1B show that the AuNPs exhibited intense absorption at 519 nm and the absorption peak underwent a red shift of 4 nm due to DNA modification. The increase in negative charge determined by DLS (Fig. S1A†) further confirmed that thiolated DNA was successfully conjugated to AuNPs.

The CdTe:Zn^{2+} DNA-QDs emitted strong fluorescence with the maximum emission wavelength at 590 nm. As shown in Fig. 1C, the TEM images indicated that the DNA-QDs were well dispersed and the average diameter was 3.35 nm. The UV-vis absorption spectra in Fig. 1D display two peaks, representing DNA (260 nm) and QDs (570 nm), respectively.

The MCH/DNA-Au-QD assembly was successfully assembled and purified by centrifugation. As shown in the TEM images (Fig. 2A and B), the QDs were attached to the surface of AuNPs *via* DNA hybridization, which resulted in reduced mobility in the agarose gel electrophoresis (Fig. 2C, band 2) in comparison with that of MCH/DNA-AuNPs (Fig. 2C, band 1). The fluorescence of QDs was quenched due to nanosurface energy transfer (NSET) accompanied by a sharp decrease in the fluorescence lifetime (Table 1 and Fig. S2†). Upon the addition of target DNA, the DNA-QDs deviated from AuNPs, which led to a higher mobility of band 3 (Fig. 2C), supporting the feasibility of the sensor.

The effect of MCH treatment on the NSET-based MCH/DNA-Au-QD sensor

A nucleic acid was employed as a target DNA, as listed in Table S1.† However, the original DNA-Au-QD sensor suffered from a comparatively low fluorescence intensity and a low signal to background ratio of 2 (Fig. S3†). To this end, we looked for solutions from two aspects, one is to enhance the hybridization efficiency, and the other is to improve the fluorescence recovery ratio. Significantly, we discovered that, through the introduction of MCH, which is the most commonly used thiol blocking regent, by virtue of its strongest ability of removing nonspecific DNA adsorption,[27,33,34] both higher hybridization efficiency and a higher fluorescence recovery ratio were achieved simultaneously. As shown in Fig. 3A and B, with the increase of the MCH concentration, the background and signal both exhibited an identical trend of first increasing and then decreasing. The increase of background was due to the increase in the number of DNA-QDs loaded on DNA-AuNPs, which indicated an enhanced hybridization efficiency. And the rise in both the signal and F/F_0 was contributed by an enhanced fluorescence recovery ratio. The enhancement in hybridization efficiency could be explained by the ability of MCH in eliminating nonspecific adsorption and regulating the surface coverage of

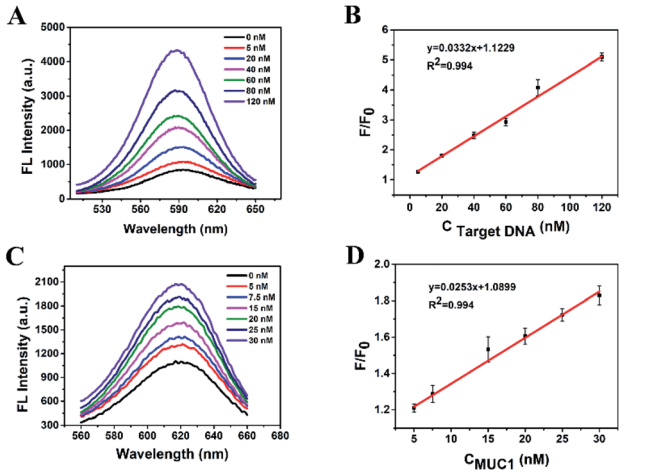

Fig. 5 Fluorescence spectra and calibration curves of the MCH/DNA-Au-QD sensor upon addition of target DNA (A and B) and MUC1 (C and D) at different concentrations.

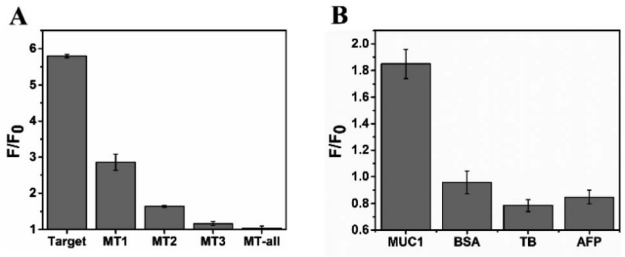

Fig. 6 Selectivity of the MCH/DNA-Au-QD sensor for the detection of (A) nucleic acid and (B) MUC1. Concentrations: target, MT1, MT2, MT3 and MT-all: 120 nM; MUC1: 30 nM; other proteins: 300 nM.

Table 2 Analytical results for the determination of MUC1 in human serum samples

	Added (nM)	Found (nM)	Mean recovery (%)	RSD (%) ($n = 3$)
0.5% serum	5	5.77	115.44	3.45
	20	19.14	95.69	1.19
	30	29.44	98.14	11.03

immobilized DNA, which has been explored in previous studies.[27,28] However, the additional effect of MCH in increasing the fluorescence recovery ratio has not been investigated yet. Firstly, we presumed that it was related to the quenching of free DNA-AuNPs to free DNA-QDs. So we mixed naked QDs with MCH/DNA-AuNPs treated with various concentrations of MCH. As displayed in Fig. 4A, the increasing FL intensity in the MCH concentration range of 0–9 μM verified our hypothesis. Hence, MCH treatment can weaken the quenching effect of free DNA-AuNPs on free QDs.

To explore the weakening of the quenching effect, several experiments were conducted. The most common quenching mechanisms between QDs and AuNPs are electrostatic interaction, inner filter effect (IFE) and NSET. The zeta potential data in Fig. S1† show that both citrate-capped AuNPs and *N*-acetyl-L-cysteine (NAC)-capped CdTe:Zn^{2+} QDs were negatively charged, and thus the electrostatic interaction was ruled out. The IFE efficiency is mainly dependent on the spectral overlap,[35] but the UV-vis peak of DNA-AuNPs (Fig. S4A†) was broadened with increasing MCH concentration, which was supposed to generate more overlapping regions along with a higher IFE efficiency. Hence, the IFE was not responsible for the effect. Then we turned our attention to NSET, which is determined by the separation distance between the donor and the acceptor surface and the spectral overlap. It is worth noting that the naked AuNPs exhibited the strongest quenching ability toward free QDs and the quenching effect was much lower after DNA modification (Fig. 4B). Given this, we speculated that the increase of the DNA layer thickness may account for the lowering of the quenching ability. The DLS results in Fig. 4C show that the average hydrodynamic diameter of DNA-AuNPs was much larger than that of naked AuNPs and displayed a trend of first increasing and then decreasing. And the electrophoresis image in Fig. 4D shows that DNA-AuNPs were retarded in the second and third bands, demonstrating the stretching of curly DNA to an upright position, which also accounted for the increase of the DNA layer thickness of DNA-AuNPs. Consequently, we concluded that the increase in the DNA layer thickness of DNA-AuNPs could enlarge the separation distance between free QDs and the DNA-AuNP surface, which lowered the NSET efficiency.

Furthermore, as shown in Table 1 and Fig. S2,† the lifetime of naked QDs was shortened from 24.67 ns to 18.22 ns in the presence of naked AuNPs, indicating the existence of nonradiative NSET. For naked QDs mixed with DNA-AuNPs, the lifetime was longer than that with naked AuNPs, and moreover, the lifetime of QDs in the presence of MCH/DNA-AuNPs was further higher. Similarly, Mukherjee reported that the modification of bulky thiolated PEG 6000 molecules on the surface of AuNPs resulted in the lowering of the long range NSET efficiency owing to the increase in the separation distance between the surface of AuNPs and free QDs, and the estimated average distance was 18.3 nm and 25.4 nm for citrate and PEG-capped AuNPs, respectively,[22] which provided further support for our conclusion.

Based on the above discussion, the variation trend of F/F_0 in Fig. 3B was influenced by the combination of hybridization efficiency and the quenching effect of free DNA-AuNPs on DNA-QDs. In the MCH concentration range of 0–9 μM, the background (F_0) increased as a result of enhanced hybridization efficiency, and the signal (F) rose sharply due to the combined effect of the weaker quenching effect and enhanced hybridization efficiency. In the range of 9–15 μM, the F_0 and F gradually reduced due to the drop in thiolated DNA. This was because the loading capacity of DNA-AuNPs with DNA-QDs was reduced due to the drop in thiolated DNA, which also led to the instability of DNA-AuNPs. In general, MCH treatment exerted a complex influence on the MCH/DNA-Au-QD sensor, and the optimal MCH concentration was 15 μM, under which the signal to background ratio was optimized to 5.7.

Analytical performance of the NSET-based MCH/DNA-Au-QD sensor

Firstly, the experimental parameters were optimized. As shown in Fig. S5,† the reaction time reached a plateau at 40 min. Since the stability of QDs was crucial to the sensor, we chose Tris–HCl buffer containing 150 mM NaCl at pH 8.3 as the reaction buffer, which was suitable for QDs. We explored the analytical performance of this improved MCH/DNA-Au-QD sensor in the detection of nucleic acids. The results in Fig. 5A and B show that the fluorescence intensity exhibited a linear relationship with the concentration of target DNA ranging from 5 nM to 120 nM, and the electrophoresis image in Fig. S6† also exhibits a higher mobility with increase in the target concentration. According to the $3\sigma/k$ rule, the limit of detection (LOD) was 1.19 nM. In contrast, for the previous sensor without MCH treatment, the signal to background ratio and fluorescence intensity were relatively low and the LOD was calculated to be 7.12 nM (Fig. S3†). Hence, after MCH treatment, the LOD for the sensor was approximately 6-fold lower than that of the original sensor, generating higher sensitivity. Obviously, the benefit of higher fluorescence recovery contributed by MCH treatment was reflected. Compared with the previous method without amplification (Table S2†), the sensitivity of this improved fluorescent sensor was superior to some of them.

Subsequently, the specificity of the sensor was investigated by using three DNA sequences, including the target DNA, the single-base mismatched target (MT1), the two-base mismatched target (MT2), the three-base mismatched target (MT3) and all-base mismatched target (MT-all) at the same concentration. As displayed in Fig. 6A, except for MT1, the F/F_0 of other mismatched targets appeared to be close to 1, showing excellent selectivity toward nucleic acids.

To further explore the universality of the improved sensor, we partially changed the DNA sequence of P1 into the aptamer of MUC1, which allowed the detection of MUC1 *via* the specific binding between MUC1 and the aptamer. As shown in Fig. 5C and D, based on the linear increase of FL intensity in response to MUC1, a calibration curve was plotted in the MUC1 concentration range of 5–30 nM, and the LOD was 1.78 nM. The specificity of the sensor was tested as shown in Fig. 6B by using five different proteins, demonstrating good specificity toward MUC1.

In order to evaluate the analytical performance of the MCH/DNA-Au-QD sensor in practical samples, the detection was performed in 0.5% human serum spiked with different concentrations of MUC1. As listed in Table 2, the recovery was in the range of 95.69–115.44% and the relative standard deviation (RSD) varied from 1.19% to 11.03%. Though the QD fluorescence was slightly affected at low concentration, this sensor showed certain advantages of short analysis time, simple operation, high universality and a wide linear range.

Conclusions

In summary, in the process of constructing MCH/DNA-Au-QD sensors, we found that MCH treatment of DNA-AuNPs weakened its quenching effect towards free QDs. The mechanism was studied and deduced to be lowering of long distance NSET efficiency induced by the increase in the separation distance of DNA-AuNPs and free QDs. Significantly, an optimized sensor performance was achieved benefiting from a higher signal to background ratio. On the one hand, this sensor can be employed for other target assays by simply altering the DNA sequence of the aptamer, making it a potential sensing candidate. On the other hand, we believe that the positive effect of MCH on the sensor provides a new research perspective for exploring NSET-based applications for better performance, which is not just meaningful for accurate spectral analysis, but also for bioimaging and other fields.

Conflicts of interest

There are no conflicts to declare.

Acknowledgements

This research was supported by the National Natural Science Foundation of China (21974101 and 21675119) and Large-scale Instrument and Equipment Sharing Foundation of Wuhan University.

Notes and references

1 C. S. Yun, A. Javier, T. Jennings, M. Fisher, S. Hira, S. Peterson, B. Hopkins, N. O. Reich and G. F. Strouse, *J. Am. Chem. Soc.*, 2005, **127**, 3115–3119.
2 C. Chen and N. Hildebrandt, *Trends Anal. Chem.*, 2020, **123**, 115748.
3 P. F. Gao, Y. F. Li and C. Z. Huang, *Trends Anal. Chem.*, 2020, **124**, 115805.
4 W. T. Yang, Y. Shen, D. Y. Zhang, C. Li, R. Yuan and W. J. Xu, *Anal. Chem.*, 2019, **91**, 7782–7789.
5 R. Y. Zhang, J. D. Sun, J. Ji, F. W. Pi, Y. Xiao, Y. Z. Zhang and X. L. Sun, *Sens. Actuators, B*, 2019, **282**, 910–916.
6 H. Y. Zou, P. F. Gao, M. X. Gao and C. Z. Huang, *Analyst*, 2015, **140**, 4121–4129.
7 M. Kalita, S. Balivada, V. P. Swarup, C. Mencio, K. Raman, U. R. Desai, D. Troyer and B. Kuberan, *J. Am. Chem. Soc.*, 2014, **136**, 554–557.
8 R. C. Qian, L. Ding, L. W. Yan, M. F. Lin and H. X. Ju, *J. Am. Chem. Soc.*, 2014, **136**, 8205–8208.
9 C. K. K. Choi, J. M. Li, K. C. Wei, Y. J. Xu, L. W. C. Ho, M. L. Zhu, K. K. W. To, C. H. J. Choi and L. M. Bian, *J. Am. Chem. Soc.*, 2015, **137**, 7337–7346.
10 M. Ku, Y. Hong, D. Heo, E. Lee, S. Hwang, J. S. Suh and J. Yang, *Biosens. Bioelectron.*, 2016, **77**, 471–477.
11 I. T. Chen, P. H. Chang, Y. C. Chang and T. F. Guo, *Sci. Rep.*, 2013, **3**, 1505.
12 Z. B. Luo, L. J. Zhang, R. J. Zeng, L. S. Su and D. P. Tang, *Anal. Chem.*, 2018, **90**, 9568–9575.
13 J. K. Vaishnav and T. K. Mukherjee, *J. Photochem. Photobiol., A*, 2020, **401**, 12.

14 K. Saha, S. S. Agasti, C. Kim, X. N. Li and V. M. Rotello, *Chem. Rev.*, 2012, **112**, 2739–2779.
15 M. Bruchez, M. Moronne, P. Gin, S. Weiss and A. P. Alivisatos, *Science*, 1998, **281**, 2013–2016.
16 Z. A. Peng and X. G. Peng, *J. Am. Chem. Soc.*, 2001, **123**, 183–184.
17 P. Wu and X.-P. Yan, *Chem. Soc. Rev.*, 2013, **42**, 5489–5521.
18 Y. Ma, G. Mao, W. Huang, G. Wu, W. Yin, X. Ji, Z. Deng, Z. Cai, X.-E. Zhang, Z. He and Z. Cui, *J. Am. Chem. Soc.*, 2019, **141**, 13454–13458.
19 C. Liu, G. Mao, C. Su, X. Ji, Z. Chen and Z. He, *Anal. Methods*, 2015, **7**, 7748–7752.
20 H. Han, V. Valle and M. M. Maye, *J. Phys. Chem. C*, 2012, **116**, 22996–23003.
21 X. Zhang, C. A. Marocico, M. Lunz, V. A. Gerard, Y. K. Gun'ko, V. Lesnyak, N. Gaponik, A. S. Susha, A. L. Rogach and A. L. Bradley, *ACS Nano*, 2012, **6**, 9283–9290.
22 J. K. Vaishnav and T. K. Mukherjee, *J. Phys. Chem. C*, 2018, **122**, 28324–28336.
23 S. Q. Chai, W. Y. Lv, J. H. He, C. H. Li, Y. F. Li, C. M. Li and C. Z. Huang, *Anal. Chem.*, 2019, **91**, 6761–6768.
24 X. He, T. Zeng, Z. Li, G. Wang and N. Ma, *Angew. Chem., Int. Ed.*, 2016, **55**, 3073–3076.
25 M. Li, Q. Y. Wang, X. D. Shi, L. A. Hornak and N. Q. Wu, *Anal. Chem.*, 2011, **83**, 7061–7065.
26 X. Wang and X. Q. Guo, *Analyst*, 2009, **134**, 1348–1354.
27 S. Park, K. A. Brown and K. Hamad-Schifferli, *Nano Lett.*, 2004, **4**, 1925–1929.
28 W. Zhao, W. Chiuman, J. C. F. Lam, S. A. McManus, W. Chen, Y. Cui, R. Pelton, M. A. Brook and Y. Li, *J. Am. Chem. Soc.*, 2008, **130**, 3610–3618.
29 S. Barbosa, A. Agrawal, L. Rodriguez-Lorenzo, I. Pastoriza-Santos, R. A. Alvarez-Puebla, A. Kornowski, H. Weller and L. M. Liz-Marzan, *Langmuir*, 2010, **26**, 14943–14950.
30 L. M. Demers, C. A. Mirkin, R. C. Mucic, R. A. Reynolds, R. L. Letsinger, R. Elghanian and G. Viswanadham, *Anal. Chem.*, 2000, **72**, 5535–5541.
31 B. W. Liu and J. W. Liu, *J. Am. Chem. Soc.*, 2017, **139**, 9471–9474.
32 W. W. Yu, L. H. Qu, W. Z. Guo and X. G. Peng, *Chem. Mater.*, 2003, **15**, 2854–2860.
33 R. Wu, L. P. Jiang, J. J. Zhu and J. Liu, *Langmuir*, 2019, **35**, 13461–13468.
34 J. Zhang, C. Song, H. Zhou, J. Jia, Y. Dai, D. Cui, L. Wang and L. Weng, *Analyst*, 2020, **145**, 1219–1226.
35 S. Chen, Y. L. Yu and J. H. Wang, *Anal. Chim. Acta*, 2018, **999**, 13–26.

